JOURNAL OF THERMOPHYSICS AND HEAT TRANSFER
Vol. 25, No. 3, July–September 2011

Numerical Simulation of Melting in Porous Media via an Interfacial Tracking Model

Qicheng Chen* and Mo Yang†
University of Shanghai for Science and Technology, 200093 Shanghai, People's Republic of China
and
Yuwen Zhang‡ and Ya-Ling He§
Xi'an Jiaotong University, 710049 Xi'an, People's Republic of China

DOI: 10.2514/1.T3693

Melting in porous media within a rectangular enclosure with the presence of natural convection is simulated using an interfacial tracking method. This method combines the advantages of both the deforming and fixed-grid methods. Convection in the liquid region is modeled using the Navier–Stokes equation with Darcy's term and Forchheimer's extension. The results are obtained by using the interfacial tracking method, which is validated by comparing with the existing experimental and numerical results. The results show that the interfacial tracing method is capable of solving natural convection-controlled melting problems in porous media at both high and low Prandtl numbers.

Nomenclature

A	=	aspect ratio, W/H
C	=	specific heat, J/kg · K
C_p	=	heat capacity, J/m^3 K
f_p	=	liquid fraction at grid point P
Gr	=	Grashof number, $g\beta\Delta TH^3/\nu_\ell^2$
g	=	gravitational acceleration, m/s^2
H	=	height of wall, m
$h_{s\ell}$	=	latent heat of fusion, J/kg
K	=	dimensionless thermal conductivities, k/k_ℓ
$\hat{K}$	=	modified dimensionless thermal conductivity
$K_{s\ell}$	=	ratio of thermal conductivities, k_s/k_ℓ
k_ℓ	=	thermal conductivity in liquid, W/m · K
Nu	=	Nusselt number at heated wall, hH/k_ℓ
P	=	dimensionless pressure, $pH^2/\rho\nu_l^2$
Pr	=	Prandtl number of liquid phase-change materials, ν_ℓ/α_ℓ
p	=	pressure, Pa
Ra	=	Rayleigh number, $Gr \cdot Pr$
S	=	dimensionless location of solid–liquid interface, s/H
Ste	=	Stefan number, $c_\ell(T_h - T_m)/h_{s\ell}$
s	=	location of solid–liquid interface, m
S^0	=	dimensionless location of solid–liquid interface at last time step
T	=	temperature, K
t	=	time, s
U	=	dimensionless velocity in x direction, uH/ν_ℓ
u	=	velocity component in x direction, m/s
U_I	=	dimensionless solid–liquid interfacial velocity, $u_I H/\nu_\ell$
u_I	=	solid–liquid interfacial velocity, m/s, $\partial s/\partial t$
V	=	dimensionless velocity in y direction, vH/ν_ℓ, or volume, m^3
v	=	velocity component in y direction, m/s
W	=	width of enclosure, m
X	=	dimensionless coordinate, x/H
x	=	dimensional coordinate, m
Y	=	dimensionless coordinate, y/H
y	=	dimensional coordinate, m
α	=	thermal diffusivity, m^2/s
γ	=	liquid fraction in Eq. (2)
δ	=	liquid fraction in Eq. (3)
ε	=	porosity
θ	=	dimensionless temperature, $(T - T_m)/(T_h - T_m)$
κ	=	permeability, m^2
μ	=	viscosity of the liquid phase-change materials, kg/ms
ν	=	kinematic viscosity, m^2/s
ρ	=	density, kg/m^3
τ	=	dimensionless time, $\nu_\ell t/H^2$
Ω	=	heat capacity ratio, $\overline{\rho c}/(\rho c)_\ell$

Subscripts

c	=	cold
E	=	east
e	=	east face of control volume
eff	=	effective
f	=	fluid
h	=	heated
I	=	interface
i	=	initial
ℓ	=	liquid
m	=	melting point
N	=	north
n	=	north face of control volume
p	=	porous matrix
ref	=	reference
S	=	south
s	=	solid
W	=	west
w	=	west face of control volume

Introduction

SOLID–LIQUID phase changes in porous media widely occur in various natural phenomena and industrial applications, including the freezing and melting of soils [1], artificial freezing of ground for mining and construction purposes [2], thermal energy storage [3],

Presented as Paper 2011-3945 at the 42nd AIAA Thermophysics Conference, Honolulu, HI, 27–30 June 2011; received 14 February 2011; revision received 8 April 2011; accepted for publication 12 April 2011.

*Graduate Student, College of Energy and Power Engineering.
†Professor and Associate Dean, College of Energy and Power Engineering.
‡Changjiang Scholar Guest Chair Professor, College of Energy and Power Engineering; Professor, Department of Mechanical and Aerospace Engineering, University of Missouri, Columbia, Missouri 65211; zhangyu@missouri.edu. Associate Fellow AIAA (Corresponding Author).
§Professor and Director, Key Laboratory of Thermal Fluid Science and Engineering of MOE.

and freezing of soil around the heat exchanger coils of a ground-based heat pump [4,5]. In the last several decades, quantitative experiments and numerical simulations were carried out by many researchers. Although the early studies about phase change in porous media treated melting and solidification as conduction controlled, the role and importance of natural convection are gradually recognized.

Since the location of the solid–liquid interface is unknown a priori, melting and solidification is referred to as moving boundary problems. A variety of numerical techniques have been developed to overcome the difficulties in handling moving boundaries: the enthalpy method [6,7], the equivalent heat capacity method [8], the isotherm migration method [9], and the coordinate transformation method [10–15]. These methods have been introduced by researchers to overcome the difficulties in handling moving boundaries. Some previous works on multidimensional moving boundary problems include those by Duda et al. [16], Saitoh [17], Gong and Mujumdar [18], Cao et al. [19], Khillarkar et al. [20], Chatterjee and Prasad , and Beckett et al. [22].

The preceding numerical models can be divided into two groups [23]: deforming grid schemes (or strong numerical solutions) and fixed-grid schemes (or weak numerical solutions). Both groups could provide reasonably accurate results [24]. Two major methods in the fixed-grid schemes are used to solve the phase-change problems: the enthalpy method [25] and the equivalent heat capacity method [26,27]. Cao and Faghri combined the advantages of enthalpy and equivalent heat capacity methods and proposed a temperature transforming model (TTM) [28]. Zhang and Faghri used TTM to study phase change in a microencapsulated phase-change materials (PCM) [29] and an externally finned tube [30].

Beckermann and Viskanta [31] propose a generalized model based on volume-averaged governing equations for melting and solidification in porous media. Later, Chang and Yang [32] proved that Beckermann and Viskanta's model [31] could handle even more complicated problems. Chakraborty and Dutta proposed a generalized formulation for evaluation of latent heat functions in enthalpy-based macroscopic models for the convection–diffusion phase-change process [33]. Pal et al. carried out an enthalpy-based simulation for the evolution of equiaxial dendritic growth in an undercooled melt of a pure substance [34]. In addition to the aforementioned macroscopic models, Chatterjee and Chakraboty also developed an enthalpy-based lattice Boltzmann model for the diffusion dominated solid–liquid phase change [35]. DasGupta et al. proposed a homogenization-based upscaling as a superior technique over the conventional volume-averaging methodologies for effective property prediction in multiscale solidification melding [36].

Zhang and Chen proposed an interfacial tracking method to solve melting and resolidification of gold film subject to nano- to femtosecond laser heating [37]. Chen et al. successfully solved natural convection-controlled melting in an enclosure at a higher Rayleigh number by using the interfacial tracking method [38]. The interfacial tracking method combined the advantages of the deforming grid and fixed-grid methods. The location of the solid–liquid interface could be obtained by energy balance at the solid–liquid interface at every time step. In this paper, the interfacial tracking method will be extended to solve melting in porous media within a rectangular enclosure with the presence of natural convection. The results obtained by using the interfacial tracking method will be compared with the existing experimental and numerical results.

Physical Model

Figure 1 shows the physical model of the problem: melting in porous media within a rectangular enclosure. The top and bottom walls are insulated, whereas the left and right walls are kept at constant temperatures at T_h and T_c, respectively. The initial temperature is equal to T_i, which is below the melting point T_m. The complicated interfacial geometries of the porous matrix and the solid and liquid phases prohibit a solution of the microscopic conservation equations for mass, momentum, and energy. Therefore, some form of a macroscopic description of the transport processes must be employed. The porosity of the porous media is defined as

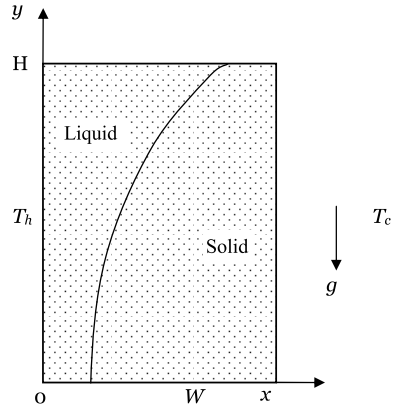

Fig. 1 Physical model.

$$\varepsilon = \frac{V_f}{V} \tag{1}$$

The liquid fraction in the pore space is defined as

$$\gamma(t) = \frac{V_\ell(t)}{V_f} \tag{2}$$

The volume fraction of liquid in the porous media is related to the porosity and liquid fraction:

$$\delta_\ell(t) = \frac{V_\ell(t)}{V} = \varepsilon\gamma(t) \tag{3}$$

The following assumptions are made:

1) The flow and heat transfer are two-dimensional and laminar.

2) The thermophysical properties of the porous matrix and the PCM are homogeneous and isotropic.

3) The porous matrix and PCM are in local thermal equilibrium.

4) The porous matrix and the solid phase of PCM are rigid (i.e., $\mathbf{u}_p = \mathbf{u}_s = 0$).

5) The porous matrix/fluid mixture is incompressible, and the Boussinesq approximation can be invoked.

6) The thermophysical properties are constants, but they are different for the porous matrix p, liquid l, and solid s phases.

7) The density change during phase change is neglected (i.e., $\rho_l = \rho_s = \rho_f$).

The dimensional governing equations are as follows:

The continuity equation is

$$\frac{\partial u_\ell}{\partial x} + \frac{\partial v_\ell}{\partial y} = 0 \tag{4}$$

The momentum equation is :

$$\frac{\rho_\ell}{\delta_\ell}\frac{\partial u_\ell}{\partial t} + \frac{\rho_\ell}{\delta_\ell^2}\left(u_\ell\frac{\partial u_\ell}{\partial x} + v_\ell\frac{\partial u_\ell}{\partial y}\right) = -\frac{\partial p}{\partial x} + \frac{\mu_\ell}{\delta_\ell}\left(\frac{\partial^2 u_\ell}{\partial x^2} + \frac{\partial^2 u_\ell}{\partial y^2}\right) - u_\ell\left[\frac{\mu_\ell}{\kappa} + \frac{\rho C}{\sqrt{\kappa}}(u_\ell^2 + v_\ell^2)^{1/2}\right] \tag{5}$$

$$\frac{\rho_\ell}{\delta_\ell}\frac{\partial v_\ell}{\partial t} + \frac{\rho_\ell}{\delta_\ell^2}\left(u_\ell\frac{\partial v_\ell}{\partial x} + v_\ell\frac{\partial v_\ell}{\partial y}\right) = -\frac{\partial p}{\partial y} + \frac{\mu_\ell}{\delta_\ell}\left(\frac{\partial^2 v_\ell}{\partial x^2} + \frac{\partial^2 v_\ell}{\partial y^2}\right) - v_\ell\left[\frac{\mu_\ell}{\kappa} + \frac{\rho C}{\sqrt{\kappa}}(u_\ell^2 + v_\ell^2)^{1/2}\right] - \rho g\beta(T - T_{\text{ref}}) \tag{6}$$

where u_ℓ and v_ℓ are the intrinsic phase-averaged velocity of the liquid. The first- and second-order drag forces, named Dracy's term and Forchheimer's extension, are incorporated into Eqs. (5) and (6). Unlike Darcy's law that is valid for low flow velocity only, the momentum equations (5) and (6), with the Forchheimer term included, are applicable to a wide range of flow velocities, including low and high flow velocities.

The Boussinesq approximation is represented by the last term of Eq. (6). The superficial velocity is related to the pore velocity by

$$u = \delta_\ell u_\ell, \qquad v = \delta_\ell v_\ell \tag{7}$$

The permeability can be calculated from the Kozeny–Carman equation [39]

$$\kappa(\delta_\ell) = \frac{d_m^2 \delta_\ell}{175(1-\delta_\ell)^2} \tag{8}$$

where d_m is the mean diameter of the particles. The value of the coefficient C in Forchheimer's extension has been measured experimentally by Ward [40], which was found to be 0.55 for many kinds of porous media.

The energy equation is

$$\overline{\rho c}\frac{\partial T}{\partial \tau} + \rho c_\ell \left(u\frac{\partial T}{\partial x} + v\frac{\partial T}{\partial y}\right) = \frac{\partial}{\partial x}\left(k_{\text{eff}}\frac{\partial T}{\partial x}\right) + \frac{\partial}{\partial y}\left(k_{\text{eff}}\frac{\partial T}{\partial y}\right) \tag{9}$$

where $\overline{\rho c}$ is the mean thermal capacitance of the mixture:

$$\overline{\rho c} = \varepsilon \rho_f [\gamma c_\ell + (1-\gamma)c_s] + (1-\varepsilon)\rho_p c_p \tag{10}$$

It should be noted that, in the liquid region, $\gamma = 1$ and $\delta = \varepsilon$. On the other hand, in the pure solid region, both γ and δ are zero.

The effective thermal conductivity k_{eff} depends on the structure of the porous media. Veinberg [41] proposed a nonlinear equation, which he claimed to be universally applicable for a media with randomly distributed spherical inclusions

$$k_{\text{eff}} + \varepsilon\left[\frac{k_p - k_f}{k_f^{1/3}}\right]k_{\text{eff}}^{1/3} - k_p = 0 \tag{11}$$

where

$$k_f = \gamma k_\ell + (1-\gamma)k_s \tag{12}$$

is the thermal conductivity of the PCM.

The boundary conditions of Eqs. (4–6) and (9) are

the left vertical wall,

$$x = 0, \qquad T = T_h, \qquad u_\ell = 0, \qquad v_\ell = 0 \tag{13}$$

the right vertical wall,

$$x = W, \qquad T = T_c, \qquad u_\ell = 0, \qquad v_\ell = 0 \tag{14}$$

the bottom horizontal wall,

$$y = 0, \qquad \frac{\partial T}{\partial y} = 0, \qquad u_\ell = 0, \qquad v_\ell = 0 \tag{15}$$

the top horizontal wall,

$$y = H, \qquad \frac{\partial T}{\partial y} = 0, \qquad u_\ell = 0, \qquad v_\ell = 0 \tag{16}$$

and the melting front,

$$x = s, \qquad T = T_m \tag{17}$$

$$x = s, \qquad \left[1 + \left(\frac{\partial s}{\partial y}\right)^2\right]\left[k_{\ell,\text{eff}}\frac{\partial T_\ell}{\partial x} - k_{s,\text{eff}}\frac{\partial T_s}{\partial x}\right] = \delta_\ell \rho_\ell h_{s\ell}\frac{\partial s}{\partial t} \tag{18}$$

We introduce the following nondimensional variables:

$$X = \frac{x}{H}, \qquad Y = \frac{y}{H}, \qquad S = \frac{s}{H}, \qquad U_\ell = u_\ell \frac{H}{\nu_\ell}$$
$$V_\ell = v_\ell \frac{H}{\nu_\ell}, \qquad P = \frac{pH^2}{\rho \nu_\ell^2}, \qquad \tau = t\frac{\nu_\ell}{H^2}, \qquad \theta = \frac{T - T_m}{T_h - T_m}$$
$$K_{\ell,\text{eff}} = \frac{k_{\ell,\text{eff}}}{k_\ell}, \qquad K_{s,\text{eff}} = \frac{k_{s,\text{eff}}}{k_\ell}, \qquad Ste = \frac{c_\ell(T_h - T_m)}{h_{s\ell}}$$
$$Sc = \frac{T_c - T_m}{T_h - T_c}, \qquad Da = \frac{\kappa(\varepsilon)}{H^2}, \qquad \Omega = \frac{\overline{\rho c}}{(\rho c)_\ell} \tag{19}$$

The governing equations can be nondimensionalized as

$$\frac{\partial U_\ell}{\partial X} + \frac{\partial V_\ell}{\partial Y} = 0 \tag{20}$$

$$\left[\frac{1}{\delta}\frac{\partial U_\ell}{\partial \tau} + \frac{1}{\delta^2}\left(U_\ell\frac{\partial U_\ell}{\partial X} + V_\ell\frac{\partial U_\ell}{\partial Y}\right)\right] = \frac{1}{\delta}\left(\frac{\partial^2 U_\ell}{\partial X^2} + \frac{\partial^2 U_\ell}{\partial Y^2}\right) - U_\ell\left(\frac{\kappa}{Da} + \frac{\kappa^{1/2}C}{Da^{1/2}}(U_\ell^2 + V_\ell^2)^{1/2}\right) \tag{21}$$

$$\left[\frac{1}{\delta}\frac{\partial V_\ell}{\partial \tau} + \frac{1}{\delta^2}\left(U_\ell\frac{\partial V_\ell}{\partial X} + V_\ell\frac{\partial V_\ell}{\partial Y}\right)\right] = \frac{1}{\delta}\left(\frac{\partial^2 V_\ell}{\partial X^2} + \frac{\partial^2 V_\ell}{\partial Y^2}\right) - V_\ell\left(\frac{\kappa}{Da} + \frac{\kappa^{1/2}C}{Da^{1/2}}(U_\ell^2 + V_\ell^2)^{1/2}\right) + Gr\theta \tag{22}$$

$$\Omega\frac{\partial \theta}{\partial \tau} + U_\ell\frac{\partial \theta}{\partial X} + V_\ell\frac{\partial \theta}{\partial Y} = \frac{K_{\text{eff}}}{Pr}\left(\frac{\partial^2 \theta}{\partial X^2} + \frac{\partial^2 \theta}{\partial Y^2}\right) \tag{23}$$

where Gr is the Grashof number based on the height of the enclosure:

$$Gr = g\beta\Delta T H^3/\nu^2$$

The nondimensional boundary conditions of Eqs. (20–23) are

$$X = 0, \qquad \theta = 1, \qquad U_\ell = 0, \qquad V_\ell = 0 \tag{24}$$

$$X = 0, \qquad \theta = -Sc, \qquad U_\ell = 0, \qquad V_\ell = 0 \tag{25}$$

$$Y = 0, \qquad \frac{\partial \theta}{\partial Y} = 0, \qquad U_\ell = 0, \qquad V_\ell = 0 \tag{26}$$

$$Y = 1, \qquad \frac{\partial \theta}{\partial Y} = 0, \qquad U_\ell = 0, \qquad V_\ell = 0 \tag{27}$$

$$X = S, \qquad \theta = 0 \tag{28}$$

$$\frac{\delta_\ell}{K_{\ell,\text{eff}}}\frac{Ste}{Pr}\left[1 + \left(\frac{\partial S}{\partial Y}\right)^2\right]\left[\frac{\partial \theta_\ell}{\partial X} - \frac{K_{s,\text{eff}}}{K_{\ell,\text{eff}}}\frac{\partial \theta_s}{\partial X}\right] = U_I \tag{29}$$

Numerical Procedures and Method

Discretization of Governing Equations

The preceding two-dimensional governing equations are discretized by using a finite volume method [42]. The conservation laws are applied over a finite-sized control volume around grid points, and the governing equations are then integrated over the control volume. Staggered grid arrangement is used in the discretization of the computational domain in the momentum equations. A power law scheme is used to discretize convection/diffusion terms in the momentum and energy equations. The algebraic equation resulting from this control-volume approach is in the form of

$$a_P\phi_P = \sum a_{nb}\phi_{nb} + b \tag{30}$$

where ϕ_P represents the value of general variable ϕ (U, V, or θ) at grid point P, ϕ_{nb} are the values of the variable at P neighbor grid points, and a_P, a_{nb}, and b are corresponding coefficients and terms derived from original governing equations. The numerical simulation is accomplished by using the SIMPLE algorithm [42]. The velocity-correction equations for corrected U and V in the algorithm are

$$U_e = U_e^* + d_e(P'_P - P'_E) \tag{31}$$

$$V_n = V_n^* + d_n(P'_P - P'_N) \tag{32}$$

where e and n represent the control-volume faces between grid P and its east neighbor E, and grid P and its north neighbor N, respectively. In this work, the governing equations are used for the entire computational domains. The velocity in the solid region is set to zero by letting $a_p = 10^{20}$ and $b = 0$ in Eq. (30) for the momentum equation.

Interfacial Tracking Method

Wang and Matthys [43] proposed an effective interface-tracking method by introducing an addition node at the interface, which divides the control volume containing the interface into two small control volumes. In this work, an interfacial tracking method [37] that was developed for conduction-controlled melting of metal film under irradiation of a femtosecond laser will be extended to be able to handle the convection-controlled solid–liquid phase-change problem. This method is an alternative approach that does not require dividing the control-volume-containing interface but can still accurately account for the energy balance at the interface. For the control volume that contains a solid–liquid interface, the dimensionless temperature θ_P is numerically set as the interfacial temperature ($\theta_I = 0$) by letting $a_P = 10^{20}$ and $b = 0$ in Eq. (30) with $\phi = \theta$.

The preceding treatment yields an accurate result when the solid–liquid interface is exactly at grid point P, as shown in Fig. 2a. When the interfacial location within the control volume is not at grid point P, there are two scenarios, as shown in Fig. 2b: the interface is on the right side of the grid point, or Fig. 2c the interface is on the left side of the grid point.

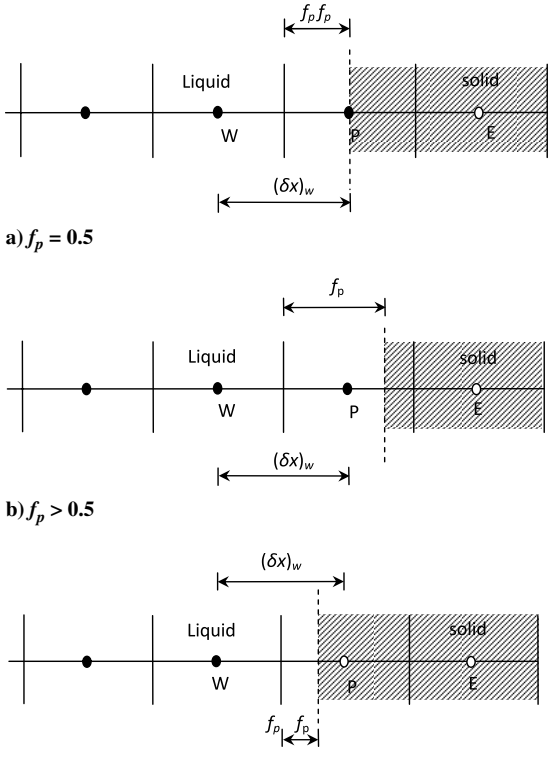

Fig. 2 Grid system near liquid–solid interface.

With the scenarios in Figs. 2b and 2c, a modified dimensionless thermal conductivity $\hat{K}_w$ at the face of the control volume w is introduced by equating the actual heat flux across the face of the control volume w, based on the position and temperature of the main grid point P [44]:

$$\frac{K_w(\theta_W - \theta_I)}{(\delta X)_w + (f_P - 0.5)(\Delta X)_P} = \frac{\hat{K}_w(\theta_W - \theta_P)}{(\delta X)_w} \tag{33}$$

Considering $\theta_P = \theta_I$, Eq. (33) becomes

$$\hat{K}_w = \frac{(\delta X)_w}{(\delta X)_w - (0.5 - f_P)(\Delta X)_P} K_w \tag{34}$$

Similarly, a modified thermal conductivity at face e of the control volume can be obtained as

$$\hat{K}_e = \frac{(\delta X)_e}{(\delta X)_e + (0.5 - f_P)(\Delta X)_P} K_e \tag{35}$$

The modified thermal conductivities defined by Eqs. (34) and (35) are used to obtain the coefficients for grid points W and E, which allows the temperature at the main grid P to be used in the computation, regardless of the location of the interface within the control volume. To determine the interfacial location, the energy balance at the interface [Eq. (29)] can be discretized and the solid–liquid interfacial velocity can be obtained as

$$U_I = \frac{Ste}{Pr}\left[1 + \left(\frac{S - S_S}{(\delta Y)_s}\right)^2\right]\left[\frac{K_w(\theta_W - \theta_I)}{(\delta X)_w - (0.5 - f_P)(\Delta X)_P} - \frac{K_e(\theta_I - \theta_E)}{(\delta X)_e + (0.5 - f_P)(\Delta X)_P}\right] \tag{36}$$

where S_S is the interfacial location at the grid at the south of grid P.

The interfacial location is then determined using

$$S = S^0 + U_I \Delta\tau \tag{37}$$

and the liquid fraction in the control volume that contains the interface is

$$f = \frac{S - X_P - (\Delta X)_P/2}{(\Delta X)_P} \tag{38}$$

Numerical Solution Procedure

The numerical solution starts from time $\tau = 0$. Once the temperature at the first control volume from the heated surface obtained exceeds the melting point, the temperature of the first control volume sets at the melting point by letting $a_P = 10^{20}$ and $b = 0$ in Eq. (29) with $\phi = \theta$. After melting is initiated, the following iterative procedure is employed to solve for the interfacial velocity and the interfacial location at each time step:

1) Assume an interface velocity U_I using the velocity U_I of the last time step as the initial value.

2) Determine the new interface location S from Eq. (37).

3) Obtain the modified dimensionless thermal conductivity, $\hat{K}_w$ and $\hat{K}_e$, at the faces of the control volume w and e from Eqs. (34) and (35).

4) Solve Eqs. (20–23) to obtain the temperature distributions and obtain the new interface velocity U_I by using Eq. (36).

5) Compare the newly obtained U_I and the assumed value in step 1. If the difference is less than 10^{-5} and the maximum difference between the temperatures obtained from two consecutive iterative steps is less than 10^{-5}, the interfacial location for the current step is obtained. If not, the process is repeated until the convergence criterion is satisfied. To obtain a converged solution of the flowfield, underrelaxation was employed for velocity and pressure and the

underrelaxation factors for velocity and pressure are 0.5 and 0.8, respectively.

The interfacial tracking method developed in this paper eliminated the need for assuming the range of phase-change temperature in other fixed-grid methods, like the equivalent heat capacity method or TTM. It does not produce nonlinear oscillation on the temperature and interfacial location like enthalpy and equivalent heat capacity methods.

Results and Discussion

The interfacial tracking method will be validated by comparing its results with experimental results as well as other numerical results. The numerical simulation of melting of gallium saturated in packed glass beads is performed first under conditions that are the same as the experiments carried out by Beckermann and Viskanta [31]. The top and bottom walls were constructed of phenolic plates, while the vertical front and back walls were made of Plexiglas. The two vertical sidewalls, which served as the heat source or sink, were multipass heat exchangers machined out of a copper plate. The heat exchangers were connected through a valve system to two constant temperature baths. Through an appropriate valve setting, the vertical sidewalls could be maintained at a constant temperature. The left wall was kept at a high constant dimensionless temperature of $T_h = 0.6$ and a low constant dimensionless temperature equal to the subcooling parameter, $Sc = 0.4$. The Rayleigh number is 8.409×10^5, the Stefan number is 0.1241, the Prandtl number is 0.0208, the Darcy number is 1.37×10^{-5}, $A = 1.0$, and the heat capacity ratios in liquid and solid are $\Omega = 0.864$ and 0.8352, respectively. The dimensionless thermal conductivities used the same value in the liquid and solid phases, $K_{\text{eff}} = 0.27$. After the grid number and time-step test, the grid number used in the simulation was 40×40 and the dimensionless time step was 2×10^{-5}. Figure 3 shows the positions of melting fronts obtained by the interfacial tracking method compared with the experiment by Beckermann and Viskanta [31] at different dimensionless times. At the early time, the present melting interfacial velocity is faster than the experimental result near the top of the enclosure; however, the melting interfacial velocity obtained by the interfacial tracking method is closer to the numerical results obtained by Beckermann and Viskanta [31]. The melting front is almost parallel to the heated wall, which indicates that the process is dominated by conduction at the early stage. As time progresses, the melting front gradually exhibits shapes that are typical for the convection-controlled melting process. At a later time, the interface becomes more inclined as the melting continues toward a steady state, whereas a good agreement between the numerical and experimental results can also be observed. At a longer time of $\tau = 0.152$, the interfacial tracking method gives results very close to the experimental results and numerical results. The difference between the predicted and measured interface position is less than 1%.

Figures 4 and 5 show the streamlines at different dimensionless times of $\tau = 0.038$ and $\tau = 0.152$, respectively. The streamlines at $\tau = 0.038$, shown in Fig. 4, indicate that the liquid is heated by the left wall and rises toward the top wall, which causes fast melting of the top portion of the PCM. When dimensionless time $\tau = 0.152$, the melting process nearly reached steady state, shown in Fig. 5.

Figures 6 and 7 show the temperature profiles at different heights in the enclosure. As shown in Fig. 6, the temperature profiles at different heights are very close to each other at the early time of $\tau = 0.038$, because the melting is driven by conduction in the liquid region. At dimensionless time $\tau = 0.152$, shown in Fig. 7, the temperature profiles at different heights become very different from each other, because the effect of convection becomes stronger as time progresses. The convection causes the temperature of the top point to be much higher than that of the bottom point. Figures 6 and 7 reveal the excellent agreement between the results from the interfacial tracking method and the results from Beckermann and Viskanta's numerical simulation [31]. The difference between the temperatures obtained by the present paper and [31] is less than 1% at any point and any time.

The preceding comparisons show that the present method of the phase-change process is well suited for simulating melting in a porous medium.

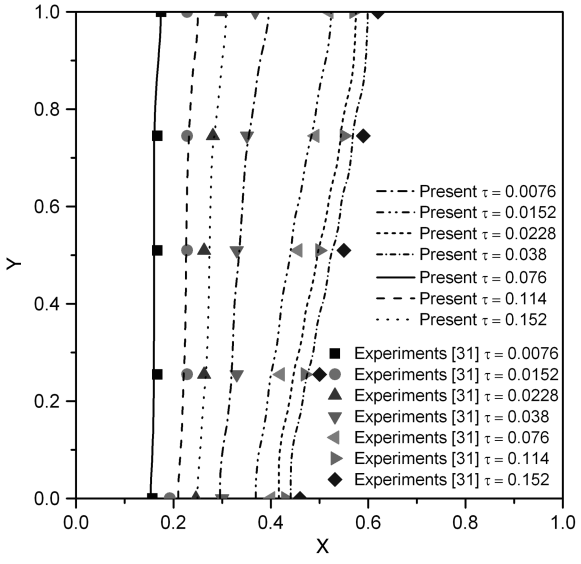

Fig. 3 Comparison of locations of melting fronts ($Ra = 8.04 \times 10^5$, $Pr = 0.0208$).

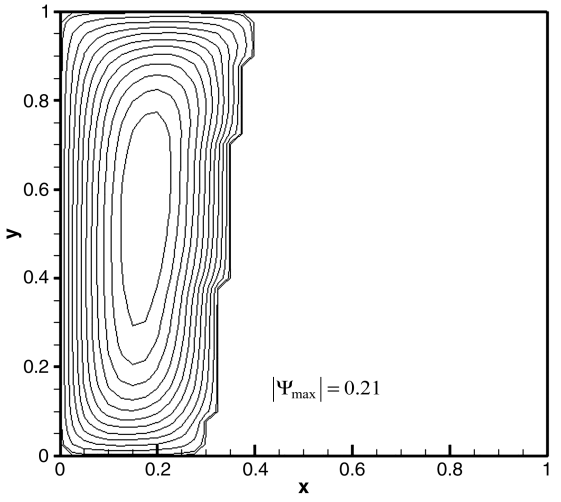

Fig. 4 Streamlines at $\tau = 0.0038$ ($Ra = 8.04 \times 10^5$, $Pr = 0.0208$).

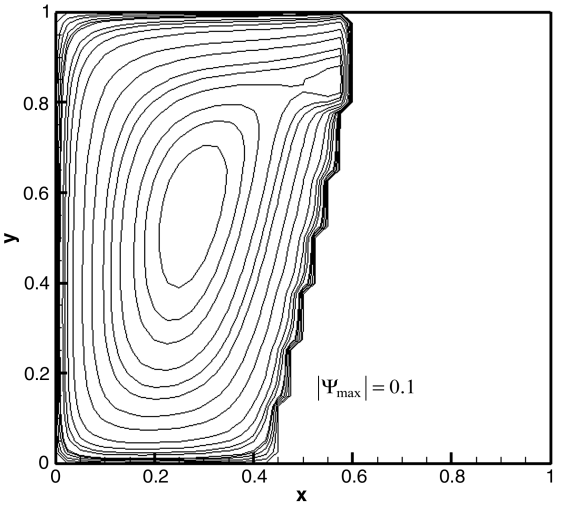

Fig. 5 Streamlines at $\tau = 0.152$ ($Ra = 8.04 \times 10^5$, $Pr = 0.0208$).

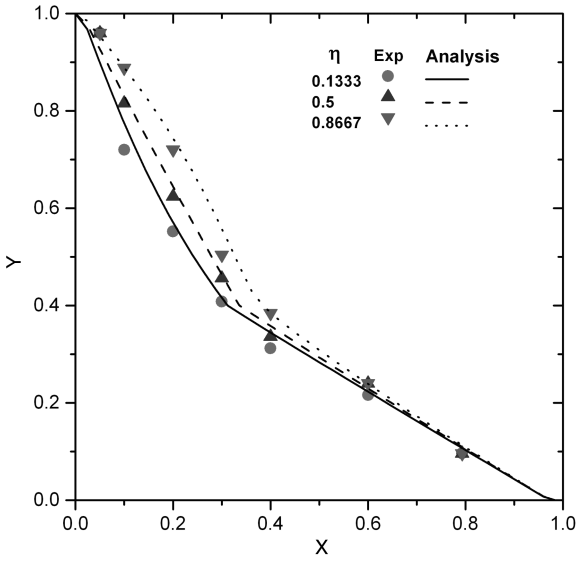

Fig. 6 Temperature profiles at $\tau = 0.0038$ ($Ra = 8.04 \times 10^5$, $Pr = 0.0208$).

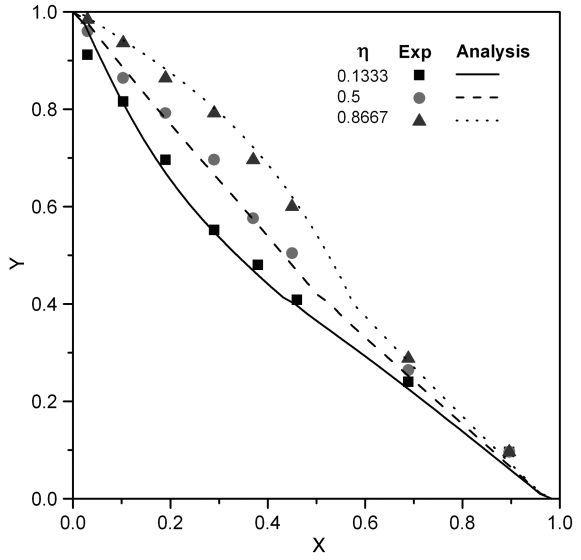

Fig. 7 Temperature profiles at $\tau = 0.152$ ($Ra = 8.04 \times 10^5$, $Pr = 0.0208$).

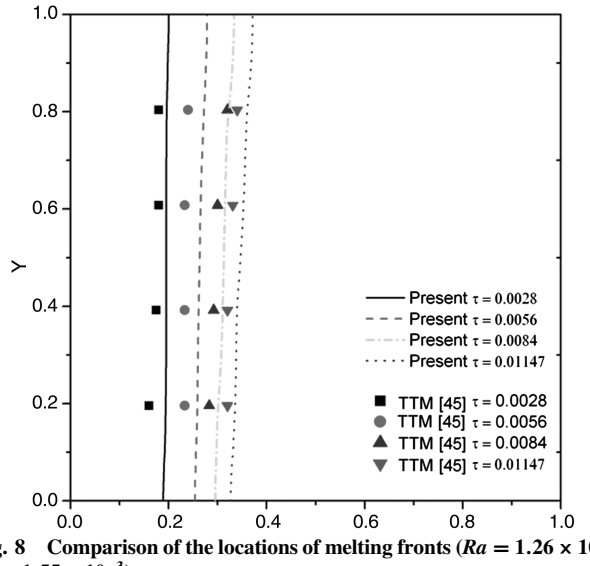

Fig. 8 Comparison of the locations of melting fronts ($Ra = 1.26 \times 10^6$, $Pr = 1.55 \times 10^{-3}$).

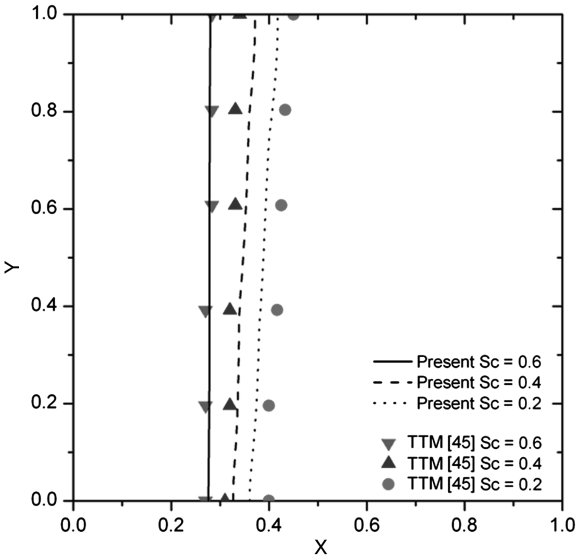

Fig. 9 Effects of subcooling number on melting process ($Ra = 1.26 \times 10^6$, $Pr = 1.55 \times 10^{-3}$).

To make sure that the interfacial tracking method is also valid at a low Prandtl number in a porous medium, an additional numerical simulation was performed based on the conditions specified by Damronglerd and Zhang [45]. The aspect ratio of the enclosure is $A = 1$. The subcooling parameter is equal to 0.4, the Rayleigh number is 1.28×10^6, the Stefan number is 0.0295, the Prandtl number is 1.55×10^{-3}, $K_{s,\text{eff}}$ is 0.414, $K_{l,\text{eff}}$ is 0.402, and ε is 0.385. After the grid number test, the grid number used in the simulation was 40×40, and the time step was 2×10^{-6}.

Figure 8 shows the comparison between the locations of solid–liquid interfaces obtained by using the present model and the TTM used by Damronglerd and Zhang [45]. At an early dimensionless time of $\tau = 0.0028$, the agreement is very good at the bottom and top regions of the rectangular cavity. Since the Prandtl number is very low, the heat transfer in the whole liquid region is governed by conduction. As melting continues to the dimensionless time of $\tau = 0.0056$, the effect of the nature convection makes the top portion of the liquid region wider. When the dimensionless time $\tau =$ 0.01147, the effect of nature convection on the melting became stronger than any previous times. Figure 9 shows a comparison of the influence on the subcooling number on the melting process. The results show that the melting front moves faster at the low subcooling parameter, $Sc = 0.2$, and slower at the high subcooling parameter, $Sc = 0.6$.

Comparisons between all the numerical results obtained by interfacial tracking method and the modified TTM indicate that the largest difference is only 0.16%. Therefore, the interfacial tracking method also can obtain very good results, even at a lower Prandlt number during natural convection-controlled melting in porous media.

Conclusions

An interfacial tracking method for two-dimensional convection-controlled melting problems in porous media was developed. It eliminated the need for assuming the range of the phase-change temperature in other fixed-grid methods. It does not produce non-linear oscillation on the temperature and interfacial location like enthalpy and equivalent heat capacity methods. Comparison between the results obtained by the present interfacial tracking method, Beckermann and Viskanta's enthalpy method [31], and Damronglerd and Zhang's TTM [45] shows that the interfacial tracking method

could be used to solve the solid–liquid phase change in porous media in wide ranges of Rayleigh and Prandtl numbers.

Acknowledgments

Support for this work by the U.S. National Science Foundation under grant number CBET-0730143 and the Chinese National Natural Science Foundation under grant numbers 50828601 and 51076105 is gratefully acknowledged.

References

[1] Miller, R. D., "Freezing Phenomena in Soils," *Applications of Soil Physics*, Academic Press, New York, 1980, pp. 254–318.

[2] Sanger, F. J., "Ground Freezing in Construction," *Journal of the Soil Mechanics and Foundations Division*, Vol. 94, 1968, pp. 131–158.

[3] "Seasonal Thermal Energy Storage," *Mechanical Engineering*, Vol. 105, No. 3, 1983, pp. 28–34.

[4] Metz, P. D., "A Simple Computer Program to Model Three-Dimensional Underground Heat Flow with Realistic Boundary Conditions," *Journal of Solar Energy Engineering*, Vol. 105, No. 1, 1983, pp. 42–49. doi:10.1115/1.3266345

[5] Svec, O., Goodrish, L. E., and Planar, J. H. L., "Heat Transfer Characteristics of In-Ground Heat Exchange," *Transactions of the ASME. Journal of Energy Resources Technology*, Vol. 7, No. 3, 1983, pp. 265–278. doi:10.1002/er.4440070307

[6] Shamsundar, N., and Sparrow, E. M., "Effect of Density Change on Multidimensional Conduction Phase Change," *Journal of Heat Transfer*, Vol. 98, No. 4, 1976, pp. 550–557. doi:10.1115/1.3450599

[7] Crowley, A. B., "Numerical Solution of Stefan Problems," *International Journal of Heat and Mass Transfer*, Vol. 21, No. 2, 1978, pp. 215–219. doi:10.1016/0017-9310(78)90225-9

[8] Bonacina, C., Comini, G., Fasano, A., and Primicerio, M., "Numerical Solution of Phase-Change Problems," *International Journal of Heat and Mass Transfer*, Vol. 16, No. 10, 1973, pp. 1825–1832. doi:10.1016/0017-9310(73)90202-0

[9] Crank, J., and Gupta, R. S., "Isotherm Migration Method in Two Dimensions," *International Journal of Heat and Mass Transfer*, Vol. 18, No. 9, 1975, pp. 1101–1107. doi:10.1016/0017-9310(75)90228-8

[10] Hsu, C. F., Sparrow, E. M., and Patankar, S. V., "Numerical Solution of Moving Boundary Problems by Boundary Immobilization and a Control-Volume Based Finite Difference Scheme," *International Journal of Heat and Mass Transfer*, Vol. 24, No. 8, 1981, pp. 1335–1343. doi:10.1016/0017-9310(81)90184-8

[11] Sparrow, E. M., and Chuck, W., "An Implicit/Explicit Numerical Solution Scheme for Phase-Change Problems," *Numerical Heat Transfer*, Vol. 7, No. 1, 1984, pp. 1–15. doi:10.1080/01495728408961808

[12] Sparrow, E. M., Ramadhyani, S., and Patankar, S. V., "Effect of Subcooling on Cylindrical Melting," *Journal of Heat Transfer*, Vol. 100, No. 3, 1978, pp. 395–402. doi:10.1115/1.3450821

[13] Cheung, F. B., Chawla, T. C., and Pedersen, D. R., "The Effect of Heat Generation and Wall Interaction on Freezing and Melting in a Finite Slab," *International Journal of Heat and Mass Transfer*, Vol. 27, No. 1, 1984, pp. 29–37. doi:10.1016/0017-9310(84)90234-5

[14] Rattanadecho, P., "Experimental and Numerical Study of Solidification Process in Unsaturated Granular Packed Bed," *Journal of Thermophysics and Heat Transfer*, Vol. 18, No. 1, 2004, pp. 87–93. doi:10.2514/1.9155

[15] Rattanadecho, P., "The Theoretical and Experimental Investigation of Microwave Thawing of Frozen Layer Using Microwave Oven (Effects of Layered Configurations and Layered Thickness)," *International Journal of Heat and Mass Transfer*, Vol. 47, No. 5, 2004, pp. 937–945. doi:10.1016/j.ijheatmasstransfer.2003.08.019

[16] Duda, J. L., Malone, M. F., Notter, R. H., and Vrentas, J. S., "Analysis of Two Dimensional Diffusion Controlled Moving Boundary Problems," *International Journal of Heat and Mass Transfer*, Vol. 18, Nos. 7–8, 1975, pp. 901–910. doi:10.1016/0017-9310(75)90182-9

[17] Saitoh, T., "Numerical Method for Multi-Dimensional Freezing Problems in Arbitrary Domains," *Journal of Heat Transfer*, Vol. 100, No. 2, 1978, pp. 294–299. doi:10.1115/1.3450798

[18] Gong, Z.-X., and Mujumdar, A. S., "Flow and Heat Transfer in Convection Dominated Melting in a Rectangular Cavity Heated from Below," *International Journal of Heat and Mass Transfer*, Vol. 41, No. 17, 1998, pp. 2573–2580. doi:10.1016/S0017-9310(97)00374-8

[19] Cao, W., Huang, W., and Russell, R. D., "An *r*-Adaptive Finite Element Method BASED upon Moving Mesh PDEs," *Journal of Computational Physics*, Vol. 149, No. 2, 1999, pp. 221–244. doi:10.1006/jcph.1998.6151

[20] Khillarkar, D. B., Gong, Z. X., and Mujumdar, A. S., "Melting of a Phase Change Material in Concentric Horizontal Annuli of Arbitrary Cross-Section," *Applied Thermal Engineering*, Vol. 20, No. 10, 2000, pp. 893–912. doi:10.1016/S1359-4311(99)00058-7

[21] Chatterjee, A., and Prasad, V., "A Full 3-Dimensional Adaptive Finite Volume Scheme for Transport and Phase-Change Processes Part I: Formulation and Validation," *Numerical Heat Transfer. Part A, Applications*, Vol. 37, No. 8, 2000, pp. 801–821. doi:10.1080/10407780050045847

[22] Beckett, G., MacKenzie, J. A., and Robertson, M. L., "A Moving Mesh Finite Element Method for the Solution of Two-Dimensional Stefan Problems," *Journal of Computational Physics*, Vol. 168, No. 2, 2001, pp. 500–518. doi:10.1006/jcph.2001.6721

[23] Voller, V. R., "An Overview of Numerical Methods for Solving Phase Change Problems," *Advances in Numerical Heat Transfer*, Vol. 1, edited by W. J. Minkowycz, and E. M. Sparrow, Taylor and Francis, Basingestoke, England, U.K., 1997, pp. 341–380.

[24] Sasaguchi, K., Ishihara, A., and Zhang, H., "Numerical Study on Utilization of Melting of Phase Change Material for Cooling of a Heated Surface at a Constant Rate, Number," *Numerical Heat Transfer. Part A, Applications*, Part A, Vol. 29, No. 1, 1996, pp. 19–31. doi:10.1080/10407789608913776

[25] Binet, B., and Lacroix, M., "Melting from Heat Sources Flush Mounted on a Conducting Vertical Wall," *International Journal of Numerical Methods for Heat and Fluid Flow*, Vol. 10, No. 3, 2000, pp. 286–306. doi:10.1108/09615530010318017

[26] Morgan, K., "A Numerical Analysis of Freezing and Melting With Convection," *Computer Methods in Applied Mechanics and Engineering*, Vol. 28, No. 3, 1981, pp. 275–284. doi:10.1016/0045-7825(81)90002-5

[27] Hsiao, J. S., "An Efficient Algorithm for Finite Difference Analysis of Heat Transfer With Melting and Solidification," American Soc. of Mechanical Engineers Paper 84-WA/HT-42, Fairfield, NJ, 1984.

[28] Cao, Y., and Faghri, A., "A Numerical Analysis of Phase Change Problem Including Natural Convection," *Journal of Heat Transfer*, Vol. 112, No. 3, 1990, pp. 812–815. doi:10.1115/1.2910466

[29] Zhang, Y., and Faghri, A., "Analysis of Forced Convection Heat Transfer in Microencapsulated Phase Change Material Suspensions," *Journal of Thermophysics and Heat Transfer*, Vol. 9, No. 4, 1995, pp. 727–732. doi:10.2514/3.731

[30] Zhang, Y., and Faghri, A., "Heat Transfer Enhancement in Latent Heat Thermal Energy Storage System by Using an External Radial Finned Tube," *Journal of Enhanced Heat Transfer*, Vol. 3, No. 2, 1996, pp. 119–127.

[31] Beckermann, C., and Viskanta, R., "Natural Convection Solid/Liquid Phase Change in Porous Media," *International Journal of Heat and Mass Transfer*, Vol. 31, No. 1, 1988, pp. 35–46. doi:10.1016/0017-9310(88)90220-7

[32] Chang, W. J., and Yang, D. F., "Natural Convection for the Melting of Ice in Porous Media in a Rectangular Enclosure," *International Journal of Heat and Mass Transfer*, Vol. 39, No. 11, 1996, pp. 2333–2348. doi:10.1016/0017-9310(95)00310-X

[33] Chakraborty, S., and Dutta, P., "A Generalized Formulation for Evaluation of Latent Heat Functions in Enthalpy-Based Macroscopic Models for Convection-Diffusion Phase Change Processes," *Metallurgical and Materials Transactions B: Process Metallurgy and Materials Processing Science*, Vol. 32, No. 3, 2001, pp. 562–564. doi:10.1007/s11663-001-0042-6

[34] Pal, D., Bhattacharya, J., Dutta, P., and Chakraborty, S., "An Enthalpy Model for Simulation of Dendritic Growth," *Numerical Heat Transfer. Part B, Fundamentals*, Vol. 50, No. 1, 2006, pp. 59–78. doi:10.1080/10407790500292366

[35] Chatterjee, D., and Chakraborty, S., "A Hybrid Lattice Boltzmann

Model for Solid–Liquid Phase Transition in Presence of Fluid Flow," *Physics Letters A*, Vol. 351, Nos. 4–5, 2006, pp. 359–367. doi:10.1016/j.physleta.2005.11.014

[36] DasGupta, D., Basu, S., and Chakraboty, S., "Effective Property Predictions in Multi-Scale Solidification Modeling Using Homogenization Theory," *Physics Letters A*, Vol. 348, Nos. 3–6, 2006, pp. 386–396. doi:10.1016/j.physleta.2005.08.045

[37] Zhang, Y., and Chen, J. K., "An Interfacial Tracking Method for Ultrashort Pulse Laser Melting and Resolidification of a Thin Metal Film," *Journal of Heat Transfer*, Vol. 130, No. 6, 2008, Paper 062401. doi:10.1115/1.2891159

[38] Chen, Q., Zhang, Y., and Yang, M., "An Interfacial Tracking Method for Natural Convection Controlled Melting in an Enclosure," *Numerical Heat Transfer. Part B, Fundamentals*, Vol. 59, No. 3, 2011, pp. 209–225. doi:10.1080/10407790.2011.550531

[39] Faghri, A., and Zhang, Y., *Transport Phenomena in Multiphase Systems*, Elsevier, Burlington, MA, 2006, pp. 273–303.

[40] Ward, J. C., "Turbulent Flow in Porous Media," *ASCE Journal of Hydrogen Division*, Vol. 90, No. HY5, 1964, pp. 1–12.

[41] Veinberg, A. K., "Permeability, Electrical Conductivity, Dielectric Constant and Thermal Conductivity of a Medium with Spherical and Ellipsoidal Inclusions," *Soviet Physics Doklady*, Vol. 11, 1967, pp. 593–595.

[42] Pantankar, S. V., *Numerical Heat Transfer and Fluid Flow*, McGraw–Hill, New York, 1980.

[43] Wang, G. X., and Matthys, E. F., "Numerical Melting of Phase Change and Heat transfer During Rapid Solidification Processes: Use of Control Volume Integral with Element Subdivision," *International Journal of Heat and Mass Transfer*, Vol. 35, No. 1, 1992, pp. 141–153. doi:10.1016/0017-9310(92)90015-K

[44] Olsson, E. D., and Bergman, T. L., "Reduction of Numerical Fluctuations in Fixed Grid Solidification Simulations," *AIAA/ASME Thermal Physics and Heat Transfer Conference*, Seattle, WA, Vol. 130, American Soc. of Mechanical Engineers, Fairfield, NJ, June 1990, pp. 130–140.

[45] Damronglerd, P., and Zhang, Y., "Numerical Simulation of Melting in Porous Media via a Modified Temperature-Transforming Model," *Journal of Thermophysics and Heat Transfer*, Vol. 24, No. 2, 2010, pp. 340–347. doi:10.2514/1.45420